ELSEVIER

Journal of Magnetism and Magnetic Materials 170 (1997) 155–167

Journal of magnetism and magnetic materials

Crystal and magnetic structures of the ternary stannides $U_2Pd_{2+y}Sn_{1-y}$

D. Laffargue[a,b], F. Bourée[b], B. Chevalier[a,*], T. Roisnel[b], P. Gravereau[a], J. Etourneau[a]

[a] *Institut de Chimie de la Matière Condensée de Bordeaux (ICMCB), CNRS [UPR 9048], Université Bordeaux I, Avenue du Docteur A. Schweitzer, 33608 Pessac Cedex, France*

[b] *Laboratoire Léon Brillouin (CEA-CNRS), CEA/Saclay, 91191 Gif-sur-Yvette Cedex, France*

Received 12 November 1996; received in revised form 30 January 1997

Abstract

$U_2Pd_{2.25}Sn_{0.75}$ stannide, investigated by X-ray diffraction on a single crystal, adopts a structure deriving from the tetragonal U_3Si_2-type, where Pd excess atoms occupy one split position surrounding the replaced Sn site. All $U_2Pd_{2+y}Sn_{1-y}$ compounds order antiferromagnetically but their magnetic structures are dependent on the chemical composition. Neutron powder diffraction yields for $y = 0$ and $y = 0.35$ non-collinear $\boldsymbol{k} = (0, 0, 0)$ and collinear $\boldsymbol{k} = (0, 0, \frac{1}{2})$ antiferromagnetic structures with magnetic moments at $T = 1.5$ K equal to 2.20(5) and 0.90(2) μ_B/U respectively. The reduced U-magnetic moment observed for $y = 0.35$ can be correlated to an increase with y of the number of Pd atoms surrounding U ones and favouring the 5f(U)–4d(Pd) hybridization. The magnetic properties of $U_2Pd_{2.25}Sn_{0.75}$ are sample-dependent and the influence of thermal treatment on these properties is discussed (two samples were investigated).

PACS: 61.55.-h; 72.25; 75.50.-e

Keywords: Uranium; Ternary stannides; Antiferromagnetism; X-ray diffraction; Single crystal; Neutron powder diffraction

1. Introduction

The ternary stannides U_2T_2Sn, with T = 3d or 4d transition metal, crystallize in an ordered version of the tetragonal U_3Si_2-type structure [1, 2] and exhibit a great variety of magnetic properties: (i) Pauli paramagnetism for U_2Fe_2Sn and U_2Ru_2Sn [3–6]; (ii) spin fluctuations behaviour at low temperatures for U_2Co_2Sn [3, 4, 6, 7]; (iii) antiferromagnetic ordering at 25, 25 and 42 K, respectively for U_2Ni_2Sn, U_2Rh_2Sn and U_2Pd_2Sn [3, 6]. These intermetallic compounds are interesting in order to study the relationship between the magnetic state of uranium and the hybridization of its 5f-orbitals with those of the ligands T and Sn.

* Corresponding author. Tel.: + 33-5-5684-6336; fax: + 33-5-5684-2761; e-mail: chevalie@chimsol.icmcb.u-bordeaux.fr.

PII S0304-8853(97)00024-3

Recently, the evolution of the magnetic properties in the sequence $U_2Fe_2Sn \rightarrow U_2Co_2Sn \rightarrow U_2Ni_2Sn$ was explained using the augmented spherical-wave (ASW) method [8]. This work shows that the 5f(U)–3d(T) hybridization depends on the number of d electrons characterizing the T transition metal: the Fermi level is between 3d(T)-states and 5f(U)-states in U_2Fe_2Sn, at the bottom of 5f(U)-states in U_2Co_2Sn and in the 5f(U)-states in U_2Ni_2Sn. This calculation agrees with the experimental results exhibiting for 5f(U)-electrons a transition from itinerant behaviour (U_2Fe_2Sn) to a more localized one (U_2Ni_2Sn).

Among these ternary stannides, U_2Pd_2Sn shows a particular behaviour: Sn atoms can be replaced by Pd giving the $U_2Pd_{2+y}Sn_{1-y}$ solid solution with $0 \leqslant y \leqslant 0.44(2)$. These compounds order antiferromagnetically [9], with Néel temperatures T_N decreasing from 42(1) K to 13(1) K as y increases from 0 to 0.44. In the same time, the substitution of palladium for tin induces interesting variation of d_{U-U} distances: these along the c-axis increase with y whereas those existing in the basal (a, b)-plane decrease [9]. This variation responsible for the magnetic anisotropy of the 5f(U)-band could play an important role on the magnetic structure of these ternary stannides. Many works performed on equiatomic compounds UTX (T = transition metal and X = Al, Si, Ge, ...) show the relationship between the orientation of U-magnetic moment and the coordination of the actinide [10, 11]. In these compounds, U-magnetic moments are often aligned perpendicularly to the direction of smaller d_{U-U} spacing. These distances induce an increase of the 5f(U)–5f(U) hybridization leading to a compression of the 5f(U)-states along their directions; consequently, the associated orbital U-moment is oriented perpendicular to these links. From this view, it is interesting to correlate the magnetic structure of $U_2Pd_{2+y}Sn_{1-y}$ stannides with their chemical composition.

In this paper, we discuss the structural properties of $U_2Pd_{2+y}Sn_{1-y}$ compounds using our investigation by X-ray diffractometry on single-crystal for $y = 0.25$ sample. Also, the magnetic structure of stannides corresponding to $y = 0$, 0.25 and 0.35, studied by neutron powder diffraction, is discussed in relation to the evolution of interatomic distances (d_{U-U}, d_{U-Pd} and d_{U-Sn}) with composition. Of course, we consider the recent investigations performed by us [12] and Purwanto et al. [13] on the magnetic structure of U_2Pd_2Sn.

2. Experimental procedures

All the polycrystalline samples were prepared, as reported previously [9], by melting the constituent elements under a purified argon atmosphere. After melting, the samples U_2Pd_2Sn and $U_2Pd_{2.35}Sn_{0.65}$ were annealed in vacuum at 800°C for 2 weeks. Their characterization by microprobe analysis reveal a perfect chemical homogeneity for U_2Pd_2Sn and the presence of small amounts of UPd_3 in $U_2Pd_{2.35}Sn_{0.65}$.

Our investigation on $U_2Pd_{2.25}Sn_{0.75}$ stannide was performed both on a melted and quenched (as-cast) sample and on a product obtained after annealing at 800°C for 1 month. The chemical homogeneity of both samples was examined by electron microprobe. The as-cast sample shows large dispersions in the Pd and Sn distributions: some parts of the sample correspond to $U_2Pd_{2.12}Sn_{0.88}$ and others have $U_2Pd_{2.4}Sn_{0.6}$ as chemical composition. On the contrary, the homogeneity of the annealed sample is significantly improved. At this stage, a tiny single crystal was isolated by mechanical fragmentation from this sample and investigated with an automatic diffractometer using a procedure described previously [1].

Magnetization measurements were carried out using a superconducting quantum interference device (SQUID) magnetometer.

Neutron powder diffraction experiments were performed at the Orphée reactor (CEA/Saclay, France) on the two-axis diffractometers G41 ($\lambda =$ 242.6 pm; 800-cells-position-sensitive detector) and 3T2 (high-resolution powder diffractometer; $\lambda = 122.59$ pm). The data were analysed using the Rietveld profile method by the FULLPROF program [14], with neutron scattering lengths and U^{3+} magnetic form factor taken from Refs. [15, 16], respectively.

3. Results and discussion

3.1. Structural properties

3.1.1. X-ray diffraction on single crystal

Examination by X-ray photographic techniques of the $U_2Pd_{2.25}Sn_{0.75}$ single crystal confirms that the stannide adopts the tetragonal symmetry. The only systematic extinction ($0\,k\,l$ observed only for $k = 2n$) leads to the possible space groups P4bm, P$\bar{4}$b2 and P4/mbm. 3917 reflections were measured in the reciprocal space corresponding to $-14 \leqslant h \leqslant 14$, $-14 \leqslant k \leqslant 14$ and $0 \leqslant l \leqslant 7$. After application of both Lorentz and polarization corrections and averaging of the symmetry-equivalent reflections, these data lead to 375 reflections with $F_0^2 > 3\sigma(F_0^2)$ (F_0 is the observed structure factor) and to an internal inconsistency index value $R_{INT} = 8.8\%$.

Starting from the atomic positional parameters published previously for U_2Pd_2Sn [13] (space group P4/mbm), the structure of $U_2Pd_{2.25}Sn_{0.75}$ stannide was refined using the SHELX 76 program [17]. U and Pd1 atoms were located, respectively, at 4h and 4g positions whereas the excess of palladium (Pd2 atom) and Sn were randomly distributed at the 2a site. At this stage, the structure refinement performed varying the occupancy parameters between Pd2 and Sn atoms reveals the existence of strong residual electron density (48.5×10^{-6} ē pm^{-3}) located at 4e site (0; 0; ≈0.32). A similar result was recently observed during our investigation of the structural properties of the $Ce_2Pd_{2+x}Sn_{1-x}$ system [18]. In these stannides, Pd2 atoms occupy a split position 4e surrounding the replaced tin atom position (2a site) located at the center of the [Ce_8] tetragonal prism. The atomic positional parameters obtained for the prototype $Ce_2Pd_{2.14}Sn_{0.86}$ [18] were used as starting parameters for the refinement of the structure of the ternary stannide based on uranium. The final atomic coordinates, displacement parameters and conventional reliability factors are given in Table 1. Our study shows that the $U_2Pd_{2+y}Sn_{1-y}$ and $Ce_2Pd_{2+x}Sn_{1-x}$ compounds are isostructural.

From Table 1, it can be seen that the B_{33} displacement parameter along c-axis is large for Sn position. Moreover, a residual electron density 3.9×10^{-6} ē pm^{-3} located near this position at (0, 0, 0.082) site is observed after the last structure refinement. These findings, which are similar to those made for $Ce_2Pd_{2.14}Sn_{0.86}$ [18], indicate considerable defects for the Sn position. These defects are directly connected to the presence of the Pd2 atoms.

The structure of the $U_2Pd_{2+y}Sn_{1-y}$ compounds is characterized by the existence of two tetragonal prisms Sn[U_8] and Pd2[U_8] exhibiting some differences (see, for instance, Fig. 2 in Ref. [18]): Sn is located at the center of the prism whereas the Pd2 atom moves along the c-axis and draws near to one square face of the prism. For $U_2Pd_{2.25}Sn_{0.75}$, it is worthwhile noting that the shortest distance $d_{U\text{-}Pd2} = 286.1$ pm is similar to the smaller $d_{U\text{-}Pd1}$ spacing (284.7 pm) (Table 3). Another example concerning the displacement of the Pd

Table 1
Atomic coordinates and displacement parameters for $U_2Pd_{2.25}Sn_{0.75}$ (space group P4/mbm)

Atom	Site	Atomic coordinates			Occ. (%)	Displacement parameters (10^4 pm^2)				
		x	y	z		B_{11}	B_{22}	B_{33}	B_{12}	B_{eq} [b]
U	4h	0.1746(1)	0.6746(1)	½	100	0.43(1)	0.43(1)	0.59(2)	−0.03(2)	0.49(2)
Pd1	4g	0.3707(1)	0.8707(1)	0	100	0.59(2)	0.59(2)	0.85(6)	−0.19(3)	0.68(3)
Pd2	4e	0	0	0.318(2)	12.4(4)			0.04(9)[a]		
Sn	2a	0	0	0	75.2(8)	0.26(3)	0.26(3)	0.65(6)		0.39(3)
				$R = 2.4\%$; $wR = 3.8\%$						

[a] Isotropic value.
[b] Equivalent isotropic value: $B_{eq.} = \frac{1}{3}\sum_i\sum_j B_{ij}\, a_i^* a_j^* (a_i \cdot a_j)$.

atom inside a prism formed by uranium was recently claimed for UPdSn [19] which crystallizes in the hexagonal GaGeLi-type where Pd and Sn atoms are located inside a trigonal [U_6] prism. In this case also, Pd atoms are not located at the center of the prism but near one of its triangular faces; the smallest $d_{U\text{-}Pd}$ distance being equal to 293.9 pm.

3.1.2. *Neutron powder diffraction on $U_2Pd_{2+y}Sn_{1-y}$ ($y = 0$; 0.25 and 0.35)*

The structural properties of these stannides were investigated at 300 and 1.5 K. The refined structural parameters (unit cell parameters and atomic coordinates) and the resulting interatomic distances, respectively, are given in Tables 2 and 3.

Table 2
Unit cell parameters and atomic coordinates for some $U_2Pd_{2+y}Sn_{1-y}$ stannides (A and B indicate, respectively, nominal and refined composition)

Composition (y)		T (K)	Unit cell para. (pm)		Atomic coordinates			Ref.
A	B		a	c	x_U	x_{Pd1}	z_{Pd2}	
0	0	300[a]	760.3	378.5	0.1757	0.3726		[13]
	0	300	761.0	378.2	0.1766	0.3730		[b]
	0	50	758.8	377.1	0.1766	0.3732		[13]
	0	1.5	759.2	377.0	0.1758	0.3727		[b]
0.25	0.25	300[a]	750.7	388.4	0.1746	0.3707	0.318	[b]
	0.23	300	751.3	389.5	0.1754	0.3709	0.315	[b]
	0.23	1.5	748.0	389.8	0.1751	0.3710	0.332	[b]
0.35	0.34	300	748.3	393.7	0.1740	0.3708	0.317	[b]
	0.34	1.5	745.2	393.9	0.1739	0.3701	0.317	[b]

[a] Study on single crystal.
[b] This work.

Table 3
Selected interatomic distances in some $U_2Pd_{2+y}Sn_{1-y}$ stannides

y	T (K)	Interatomic distances (pm)							Ref.
		$d_{U\text{-}U}$			$d_{U\text{-}Sn}$ (4)	$d_{U\text{-}Pd1}$		$d_{U\text{-}Pd2}$	
		(2)	(1)	(4)		(2)	(4)		
0	300	378.5	378.1	396.6	338.3	284.0	300.4		[13]
	300	378.2	380.1	396.6	338.2	283.6	300.9		[a]
	50	377.1	379.0	395.4	337.2	282.9	300.0		[13]
	1.5	377.0	377.5	396.0	337.5	283.2	299.7		[a]
0.25	300[b]	388.4	370.7	392.0	338.5	284.7	301.5	286.1	[a]
	300	389.5	372.7	392.0	338.8	284.7	302.4	286.4	[a]
	1.5	389.8	370.5	390.4	337.9	284.5	301.5	283.7	[a]
0.35	300	393.7	368.3	391.4	339.4	286.6	302.2	285.8	[a]
	1.5	393.9	366.5	389.5	338.6	285.6	303.8	284.7	[a]

[a] This work.
[b] Study on single crystal.

Our study confirms that U_2Pd_2Sn crystallizes in an ordered version of the tetragonal U_3Si_2-type. The best refinements were obtained at these two temperatures with the same reliability factor ($R = 9.1\%$). The unit cell parameters decrease with temperature (Table 2) and we can note that the shortest d_{U-U} spacing is always located along the c-axis ($d_{U-U}(2)$ in Table 3). Contrary to that claimed in Ref. [13], we observe that all d_{U-U} distances decrease with temperature. But at 1.5 K, the distance along the c-axis ($d_{U-U}(2) = 377.0$ pm) is comparable to the smaller one in the (a, b)-plane ($d_{U-U}(1) = 377.5$ pm).

For the compositions $y = 0.25$ and 0.35, the structural refinements were performed using the model determined above by X-ray diffraction on single crystal. The refinement obtained at 300 and 1.5 K leads to a reliability factor of 9.9% and 8.2% for $y = 0.25$ and 9.5% and 8.9% for $y = 0.35$.

At 300 K, the a-parameter decreases whereas the c-parameter increases with rising y (Table 2). This behaviour, explained previously [3, 18], is directly connected to the crystal structure of these stannides, which can be described as a stacking of atomic planes perpendicular to the c-axis with sequence (Pd, Sn)–U–(Pd, Sn)–U–··· In this view, the a-parameter is governed by the size of the (Pd, Sn)-network, whereas the distances d_{U-Pd1} existing in the trigonal prisms [U_6] influence the variation of the c-parameter. Replacement of Sn atom by the smaller palladium Pd2 atom involves a decrease in a-parameter of the $U_2Pd_{2+y}Sn_{1-y}$ system. It is interesting to compare the evolution of d_{U-U} distances versus chemical composition (Table 3): (i) along the c-axis, ($d_{U-U}(2)$) increase with y; (ii) on the contrary, those distances located in the (a, b)-plane ($d_{U-U}(1)$ and $d_{U-U}(4)$) decrease when Sn atoms are replaced by Pd2 ones. This result induces that the shortest d_{U-U} spacing is directed along the c-axis for $y = 0$ and within the (a, b)-plane for $y = 0.25$ and 0.35. Certainly, this change which influences the direction of the strongest 5f(U)–5f(U) hybridization could play an important role in the magnetic structure of these compounds.

Contrary to the d_{U-U} distances, those occurring between U and Sn or Pd are weakly dependent on the composition (Table 3). The d_{U-Sn} spacings observed in the $U_2Pd_{2+y}Sn_{1-y}$ system are much greater than that existing in other stannides as UPdSn ($d_{U-Sn} = 314.7$ pm) [19] or USn_3 ($d_{U-Sn} = 327.1$ pm) [20]. Concerning the smallest d_{U-Pd1} or d_{U-Pd2} distances, they are shorter than that observed in UPdSn and UPd_3 compounds; d_{U-Pd} is then equal to 293.9 pm [19] and 287.8 pm, respectively [20]. This result indicates that the 5f(U)–4d(Pd) hybridization may be considered in order to explain the physical properties of the $U_2Pd_{2+y}Sn_{1-y}$ compounds. Moreover, the increase of Pd content in this system leads to an increase of the number of Pd atoms surrounding U ones. It is well known that the 5f(U)-ligands hybridization is magnified when the coordination number of U atom is increased [20].

3.2. Magnetic properties

The temperature dependence of magnetic susceptibility measured in an applied field of 0.2 T are shown in Figs. 1 and 2.

For $y = 0$, the $\chi_m = f(T)$ curve shows a maximum at 40(1) K typical of the occurrence of an antiferromagnetic ordering. The T_N value determined in the present work is in agreement with

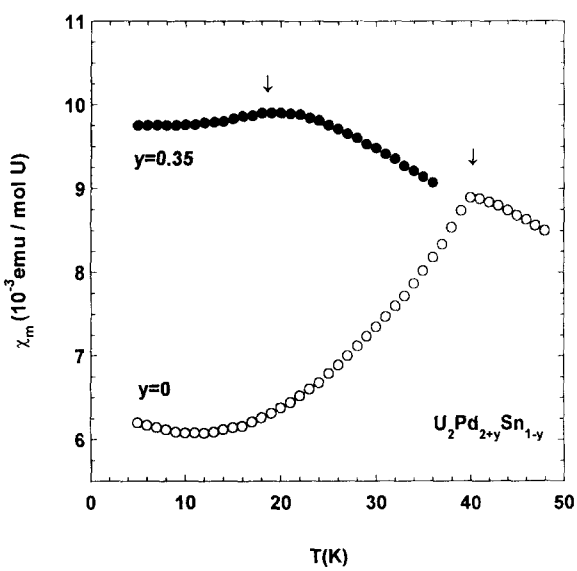

Fig. 1. Temperature dependence of the magnetic susceptibility of annealed $U_2Pd_{2+y}Sn_{1-y}$ stannides with $y = 0$ and 0.35 (the arrows show T_N temperature).

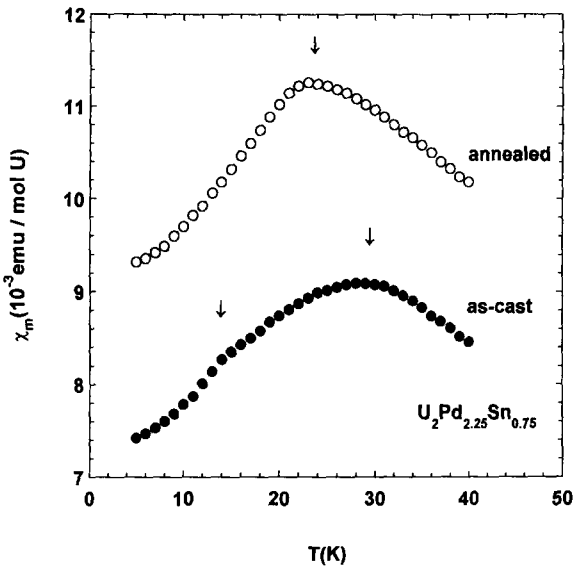

Fig. 2. Temperature dependence of the magnetic susceptibility of as-cast and annealed $U_2Pd_{2.25}Sn_{0.75}$ stannide (the arrows show T_N temperature).

previous determinations [3, 13]. The $\chi_m = f(T)$ curve relative to $y = 0.35$ exhibits near $T_N = 18(1)$ K a maximum clearly less-pronounced than that observed for $y = 0$ (Fig. 1). The origin of this last behaviour could be due to: (i) the presence of some atomic disorder induced by the substitution of Pd2 atoms for Sn creating disorder in magnetic interactions; (ii) the increase of the Kondo effect with rising y as suggested in Ref. [9] (see below). We note that T_N shifts toward the low temperatures with increasing y in the $U_2Pd_{2+y}Sn_{1-y}$ system.

The $\chi_m = f(T)$ curve of the as-cast $U_2Pd_{2.25}Sn_{0.75}$ sample reveals two anomalies (Fig. 2): a broad maximum at 29(1) K followed by a slight drop around 13(1) K. The presence of two compositions, $U_2Pd_{2.12}Sn_{0.88}$ and $U_2Pd_{2.4}Sn_{0.6}$, in this sample explains this result. It is interesting to note that the lowest T_N temperature determined here is comparable to this obtained previously for the richest palladium stannide $U_2Pd_{2.44}Sn_{0.56}$ ($T_N = 13$ K) [9]. On the contrary, only one maximum at $T_N = 23(1)$ K is detected for the annealed sample showing that the thermal treatment allows to improve its chemical homogeneity.

3.3. Magnetic structures

3.3.1. U_2Pd_2Sn

Fig. 3 shows the powder neutron diffraction patterns both in the paramagnetic state ($T = 50$ K) and in the antiferromagnetic one. At 1.5 K, four magnetic contributions appear which are indexed in the magnetic cell (a, a, c), respectively, by (2 0 0), (2 1 0), (1 0 1) and (1 1 1). The best refinement ($R_M = 8.3\%$) between observed and calculated magnetic intensities is obtained considering the magnetic model described in Fig. 4. The antiferromagnetic structure previously determined [12, 13] is therefore confirmed. The U-magnetic moments form a canted arrangement along the [1 1 0] and [1 $\bar{1}$ 0] directions, so that magnetic interactions in the (a, b)-plane are antiferromagnetic along the short $d_{U\text{-}U}(1)$ distance (Table 3). Along the c-axis, all the magnetic interactions are purely ferromagnetic.

The value of U-magnetic moment 2.20(5) μ_B at 1.5 K characterizes a nearly localized 5f(U) state in U_2Pd_2Sn, quite similar to the moment (2.05(13) μ_B/U) found in the antiferromagnet UPdSn [19]. Finally, it is interesting to note that the non-collinear magnetic structure of U_2Pd_2Sn can be explained taking into account spin–orbit coupling and an effective orbital field [21].

3.3.2. $U_2Pd_{2.35}Sn_{0.65}$

Fig. 5 shows two representative neutron powder patterns obtained, respectively, above (25 K) and below (1.5 K) its T_N temperature. We note in these patterns, a peak characteristic of the binary compound UPd_3. The presence of this impurity phase in our sample can be explained by the fact that $U_2Pd_{2+y}Sn_{1-y}$ solid solution is in balance with UPd_3 in the uranium–palladium–tin system [9]. The difference curve between 1.5 and 25 K indicates the occurrence of three additional magnetic peaks which can be indexed in the primitive nuclear cell as (1 1 $\frac{1}{2}$), (2 0 $\frac{1}{2}$) and (2 1 $\frac{1}{2}$). The magnetic structure is then described by a propagation vector $\boldsymbol{k} = (0, 0, \frac{1}{2})$. This vector characterizes other U_2T_2Sn magnetic structures such as U_2Ni_2Sn [22], U_2Ni_2In [23, 24] and U_2Rh_2Sn [23]. Magnetic group theory yields ten irreducible representations

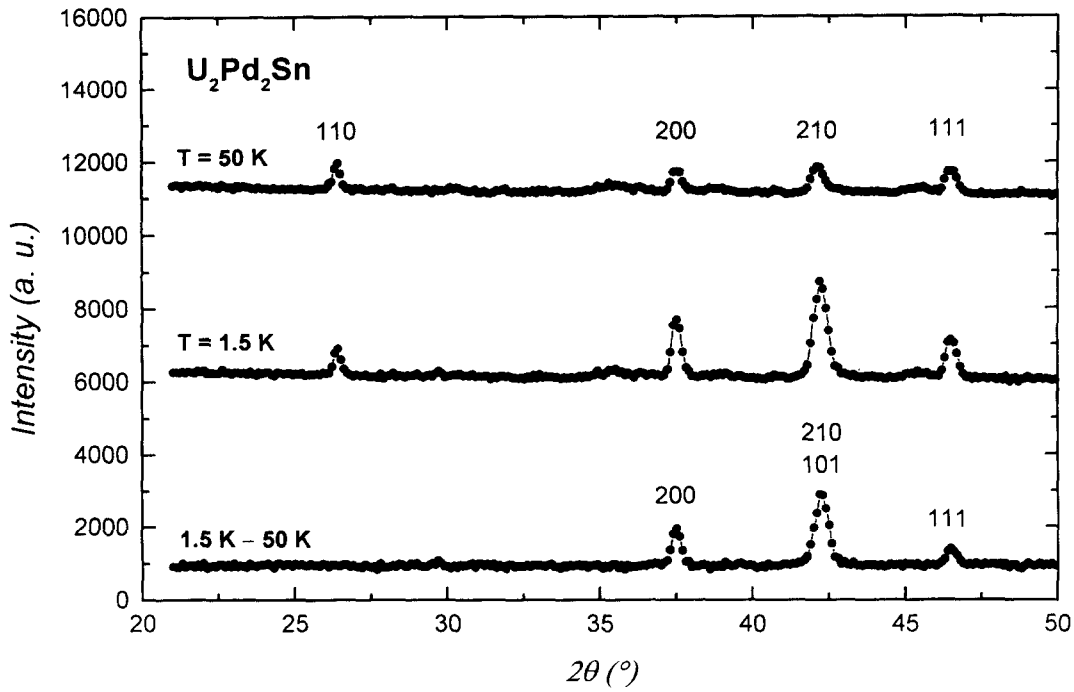

Fig. 3. Neutron diffraction patterns at 50, 1.5 K and difference for U_2Pd_2Sn.

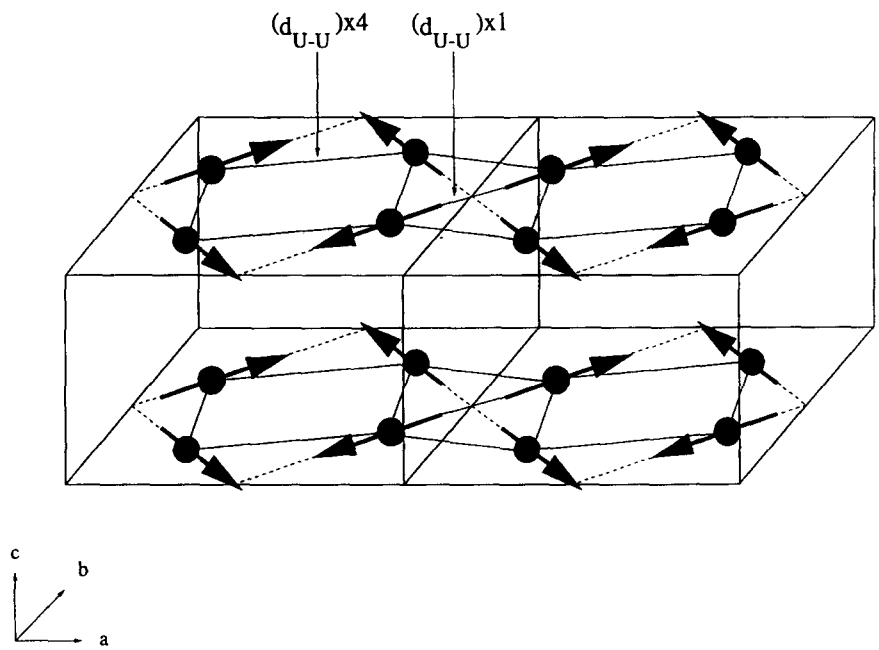

Fig. 4. Magnetic structure of U_2Pd_2Sn.

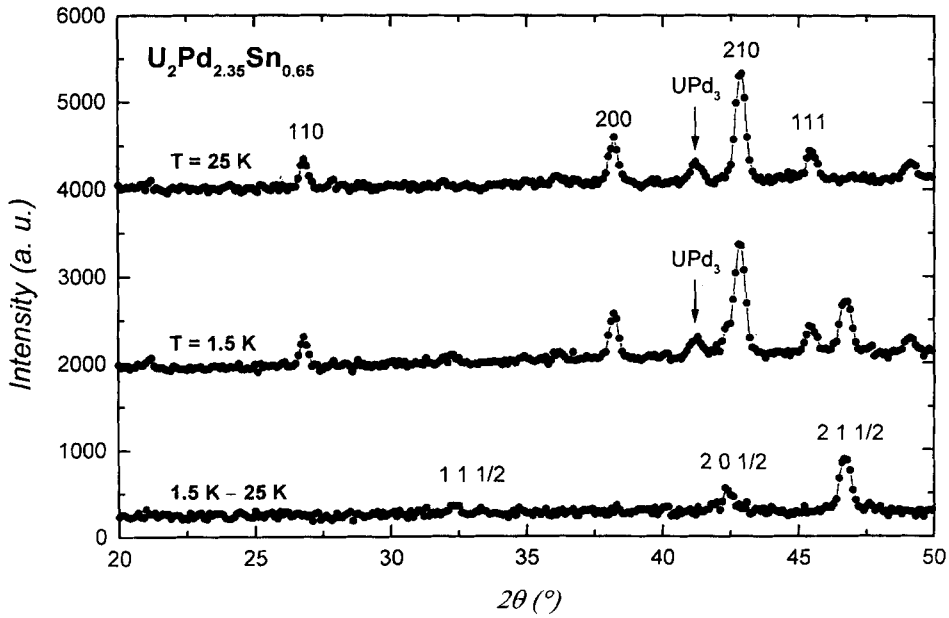

Fig. 5. Neutron diffraction patterns at 25, 1.5 K and difference for $U_2Pd_{2.35}Sn_{0.65}$.

Table 4
Experimental magnetic intensities and calculated ones for various Γ_i representations relative to $U_2Pd_{2.35}Sn_{0.65}$

$h\,k\,l$	I_{exp}	I_{calc}							
		Γ_1	Γ_2	Γ_3	Γ_5	Γ_7	Γ_8	Γ_9	Γ_{10}
1 1 ½	7.9	7.4	**10.8**	0.7	3.5	1.6	9.1	5.8	10.9
2 0 ½	30.6	6.7	**34.6**	0.4	10.2	0.3	0	6.2	0
2 1 ½	48.2	0.8	**46.8**	0.7	3.9	0.1	0.1	3.1	0.4
M (μ_B/U)		0.8(3)	**0.90(2)**	0.4(3)	1.0(2)	0.3(3)	0.5(4)	0.8(2)	0.5(4)
χ^2		10.2	**3.1**	10.6	9.8	10.7	10.5	10.0	10.5
R_M (%)		92.1	**8.2**	97.8	93.0	95.5	92.3	93.6	96.6

for the P4/mbm space group and $\boldsymbol{k} = (0, 0, \frac{1}{2})$: they are listed extensively in Ref. [22] where they are labelled $\Gamma_1,...,\Gamma_{10}$. The non-zero basis vectors of these Γ_i representations correspond to U-magnetic moments either parallel (Γ_2, Γ_8, Γ_9) or perpendicular ($\Gamma_1, \Gamma_3, \Gamma_5, \Gamma_7, \Gamma_{10}$) to the tetragonal c-axis [22].

Considering only the three magnetic reflections observed at 1.5 K, we have calculated their intensities in all the possible representations (Table 4). The best refinement ($R_M = 8.2\%$) indicates clearly the Γ_2 representation. In this case, the U-magnetic moments are directed along the c-axis: the structure is a simple stacking of ferromagnetic (0 0 1)-planes along this axis with the sequence $(+\ -\ +\ -)$ (Fig. 6). The thermal dependence of the intensity of (2 1 ½) reflection determines $T_N = 17(1)$ K as the ordering temperature (Fig. 7). This agrees with T_N value deduced from magnetization measurement (Fig. 1).

At 1.5 K, U-atoms carry a small moment (0.90(2) μ_B/U) much lower than that observed for

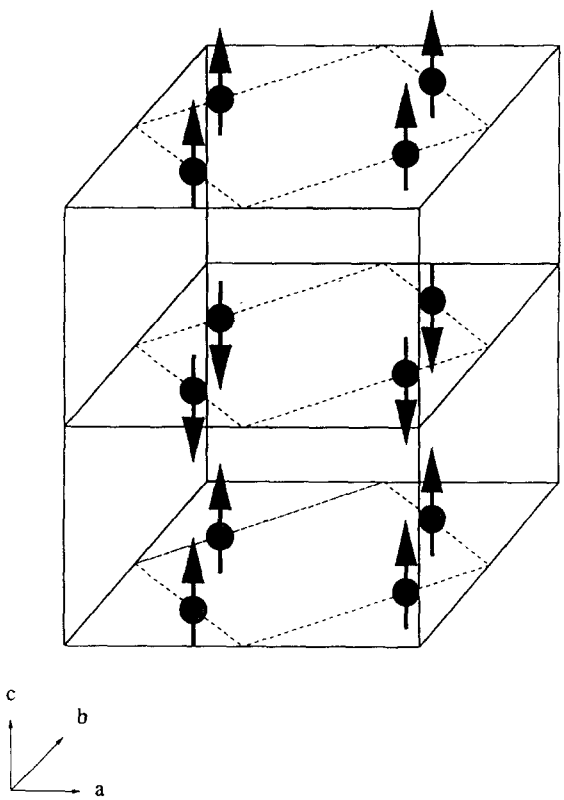

Fig. 6. Magnetic structure of $U_2Pd_{2.35}Sn_{0.65}$.

U_2Pd_2Sn. This value is comparable to that determined for U_2Ni_2Sn (1.05(5) μ_B) [22] or U_2Ni_2In (0.85(5) μ_B) [24] but greater than that measured for U_2Rh_2Sn (0.38(1) μ_B) [23] where the reduced moment is due to a strong 5f(U)-ligand hybridization. It is interesting to note that the substitution of Pd-atoms for Sn allows both: (i) an increase of the number of Pd near neighbours around uranium, (ii) the occurrence of the short $d_{U\text{-}Pd2}$ distances (Table 3). These features favour the formation of hybridized 5f(U) bands and the calculations of the densities of states (DOS) allows to say that their magnetic properties are principally governed by the strength of the 5f(U)–*n*d(T) hybridization [8]. Accordingly, the magnetic moment carried by U in this series can be correlated to the value of the $d_{U\text{-}T}$ interatomic distance. For instance, the reduction of the U-magnetic moment observed in the sequence $U_2Pd_2Sn \rightarrow U_2Rh_2Sn$, is accompanied by a decrease of the average distance $d_{U\text{-}T}$, respectively equal to 294.2 pm at 1.5 K for U_2Pd_2Sn [this work] and 288.0 pm at 30 K for U_2Rh_2Sn [23]. In this way, this distance takes in the $U_2Pd_{2+y}Sn_{1-y}$ system an almost constant value since $d_{U\text{-}Pd}$ = 294.2 and 296.4 pm at 1.5 K for $y = 0$ and 0.35, respectively, but the number of Pd atoms surrounding U increases with y: 6 (6 Pd1 atoms) for

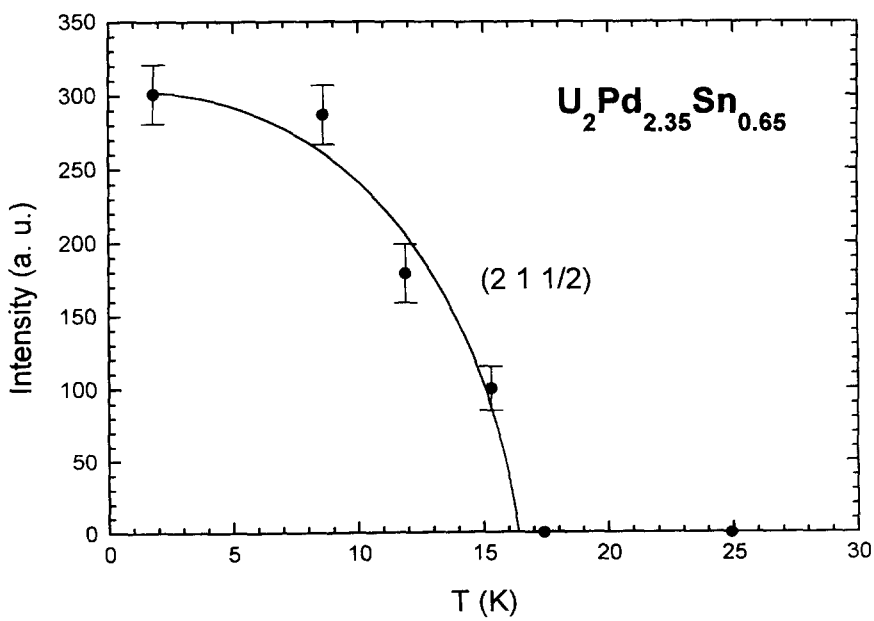

Fig. 7. Temperature dependence of the intensity of (2 1 $\frac{1}{2}$) magnetic peak in $U_2Pd_{2.35}Sn_{0.65}$.

$y = 0$ and 6.7 (6 Pd1 and 0.7 Pd2 atoms) for $y = 0.35$.

3.3.3. $U_2Pd_{2.25}Sn_{0.75}$

Figs. 8 and 9 show neutron diffraction patterns for the as-cast and annealed sample, respectively.

The difference pattern for the as-cast sample between 1.5 and 35 K reveals five additional peaks which cannot be indexed with a unique propagation vector $\boldsymbol{k}$ (Fig. 8). The peaks labelled as (2 0 0), (1 0 1) and (1 1 1) are associated to $\boldsymbol{k} = (0, 0, 0)$ whereas the others, (2 0 $\frac{1}{2}$) and (2 1 $\frac{1}{2}$), are associated to $\boldsymbol{k} = (0, 0, \frac{1}{2})$. This result suggests that the sample is highly heterogeneous and composed of two domains. In order to test this hypothesis, we have determined the temperature dependence of the intensity of two magnetic reflections characteristic of each $\boldsymbol{k}$-vector (Fig. 10): the (1 0 1) and (2, 1, $\frac{1}{2}$) peaks appear below 27(1) and 16(1) K, respectively. Moreover, no anomaly is observed near 16 K on the thermal dependence of the intensity of the (1 0 1) peak, consequently, excluding the occurrence of transition at this temperature between the magnetic structures associated to the two $\boldsymbol{k}$-vectors. On the contrary, the study confirms that the sample is heterogeneous; the magnetic peaks associated to $\boldsymbol{k} = (0, 0, 0)$ and $\boldsymbol{k} = (0, 0, \frac{1}{2})$ appear below the two T_N temperatures determined by magnetization measurements, respectively (Fig. 2).

Similar to the as-cast sample, additional lines appear in the neutron diffraction pattern measured at 1.5 K on the annealed sample (Fig. 9). These lines, characteristic of antiferromagnetic order, are indexed considering the coexistence of two types of $\boldsymbol{k}$-vector: $\boldsymbol{k} = (0, 0, 0)$ and $\boldsymbol{k} = (0, 0, \frac{1}{2})$. It is worthwhile noting that the annealing treatment of this ternary stannide induces an increase of the intensity of magnetic peaks relative to $\boldsymbol{k} = (0, 0, \frac{1}{2})$-vector. For instance, this fact is clearly illustrated by the (2 1 $\frac{1}{2}$) line which is exalted in the annealed $U_2Pd_{2.25}Sn_{0.75}$ sample (Figs. 8 and 9). This indicates that the magnetic structure of this compound adopts preferentially, as $U_2Pd_{2.35}Sn_{0.65}$, the $\boldsymbol{k} = (0, 0, \frac{1}{2})$ propagation vector. The (1 0 1) and (2 1 $\frac{1}{2}$) magnetic peaks appear together at the same temperature 17(1) K (Fig. 11), which is smaller than $T_N = 23(1)$ K determined by magnetization measurements. Certainly, only one magnetic phase ($\boldsymbol{k} = (0, 0, \frac{1}{2})$) may be detected in a sample annealed for a longer time.

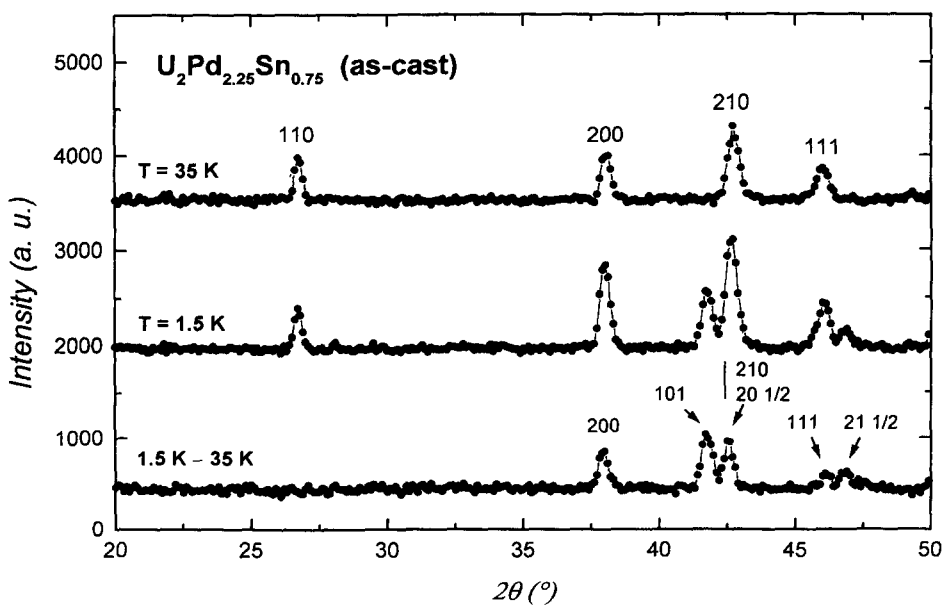

Fig. 8. Neutron diffraction patterns at 35, 1.5 K and difference for (as-cast) $U_2Pd_{2.25}Sn_{0.75}$.

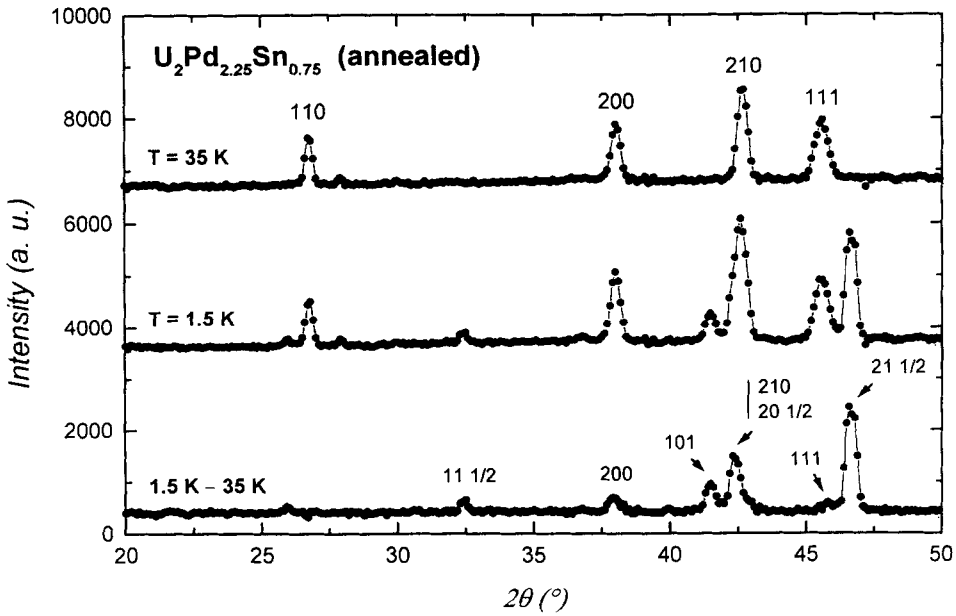

Fig. 9. Neutron diffraction patterns at 35, 1.5 K and difference for (annealed) $U_2Pd_{2.25}Sn_{0.75}$.

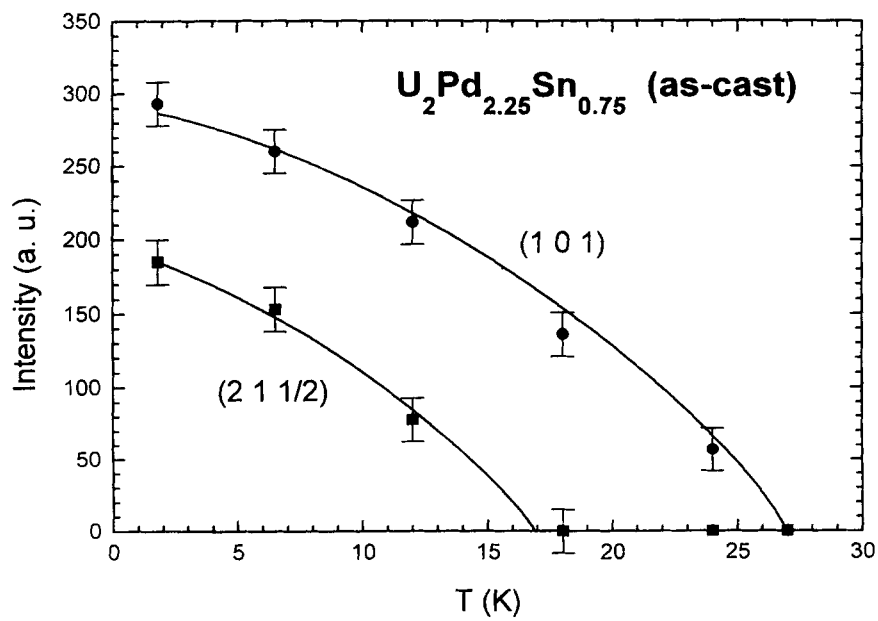

Fig. 10. Temperature dependence of the intensity of (1 0 1) and (2 1 $\frac{1}{2}$) magnetic peaks in (as-cast) $U_2Pd_{2.25}Sn_{0.75}$ sample.

4. Conclusion

The analysis at 1.5 K of the structural properties of the $U_2Pd_{2+y}Sn_{1-y}$ ternary stannides provides interesting information about the composition dependence of the d_{U-U} distances (Table 3): (i) for $y = 0$ the shortest distance within the (a, b)-basal plane ($d_{U-U}(1)$) is of the same order as

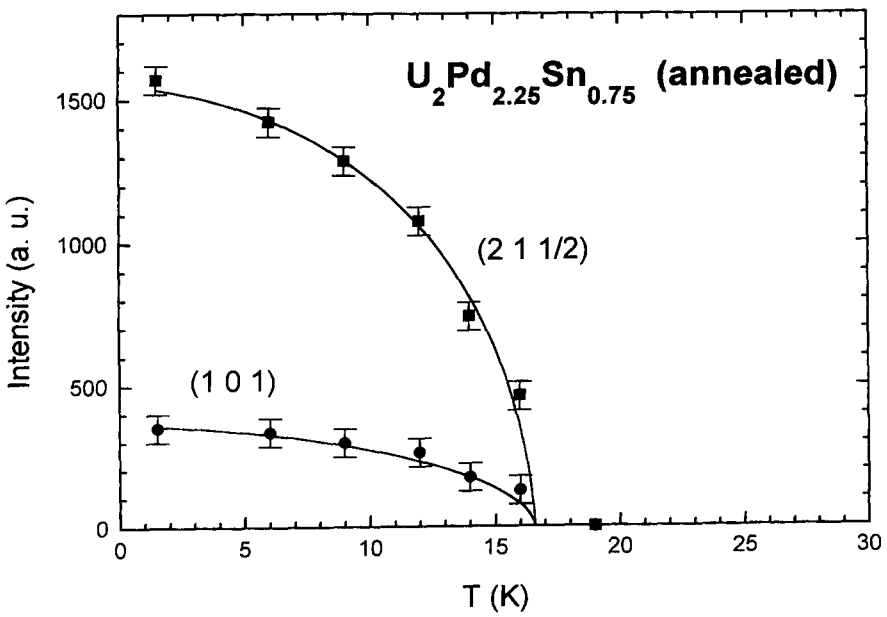

Fig. 11. Temperature dependence of the intensity of (1 0 1) and (2 1 $\frac{1}{2}$) magnetic peaks in (annealed) $U_2Pd_{2.25}Sn_{0.75}$ sample.

that existing along c-axis ($d_{U-U}(2)$); (ii) on the contrary, for higher y, $d_{U-U}(1)$ spacing is always shorter. These structural changes which influence the magnetocrystalline anisotropy involve a modification of the orientation of the U-magnetic moments. For $y = 0$ and 0.35, these moments are systematically directed perpendicularly to the shortest d_{U-U} distance: the former compound exhibits a non-collinear structure with U-moments in the (a, b)-plane whereas the latter one orders antiferromagnetically with U-moments collinear to the c-axis. The direction of the magnetic moments in $U_2Pd_{2+y}Sn_{1-y}$ system is then compatible with the empirical model developed for the UTX equiatomic compounds [10, 25].

We note that the magnetic structure of $U_2Pd_{2.35}Sn_{0.65}$ is unique among those determined recently for U_2T_2Sn stannides. Also, the reduced U-magnetic moment existing in this compound is indicative of the influence of the 5f(U)–4d(Pd) hybridization on physical properties of these compounds.

References

[1] F. Mirambet, P. Gravereau, B. Chevalier, L. Trut, J. Etourneau, J. Alloys Compounds 191 (1993) L1.
[2] M.N. Peron, Y. Kergadallan, J. Rebizant, D. Meyer, J.M. Winand, S. Zwirner, L. Havela, H. Nakotte, J.C. Spirlet, G.M. Kalvius, E. Colineau, J.L. Oddou, C. Jeandey, J.P. Sanchez, J. Alloys Compounds 201 (1993) 203.
[3] F. Mirambet, B. Chevalier, L. Fournès, P. Gravereau, J. Etourneau, J. Alloys Compounds 203 (1994) 29.
[4] B. Chevalier, P. Gravereau, L. Fournès, J. Etourneau, Proc. 5th European Conf. on Solid State Chem., Montpellier, France, 4–7 September 1995, p. 537.
[5] A.M. Strydom, P. de V. du Plessis, V.V. Gridin, Physica B 225 (1996) 89.
[6] L. Havela, V. Sechovsky, P. Svoboda, H. Nakotte, K. Prokes, F.R. de Boer, A. Seret, J.M. Winand, J. Rebizant, J.C. Spirlet, A. Purwanto, R.A. Robinson, J. Magn. Magn. Mater. 140–144 (1995) 1367.
[7] R.P. Pinto, M.M. Amado, M.A. Salgueiro, M.E. Braga, J.B. Sousa, B. Chevalier, F. Mirambet, J. Etourneau, J. Magn. Magn. Mater. 140–144 (1995) 1371.
[8] S.F. Matar, J. Magn. Magn. Mater. 151 (1995) 263.
[9] F. Mirambet, L. Fournès, B. Chevalier, P. Gravereau, J. Etourneau, J. Magn. Magn. Mater. 138 (1994) 244.
[10] L. Havela, V. Sechovsky, H. Nakotte, E. Brück, F.R. de Boer, J. Alloys Compounds 213–214 (1994) 243.

[11] J.A. Paixäo, G.H. Lander, A. Delapalme, H. Nakotte, F.R. de Boer, E. Brück, Europhys. Lett. 24 (1993) 607.
[12] F. Mirambet, D. Laffargue, F. Bourée, B. Chevalier, J. Etourneau, L. Fournès, T. Roisnel, 24ièmes Journées des Actinides, 15–19 April 1994, Obergurgl (Austria), Abstract O3.1, p. 17.
[13] A. Purwanto, R.A. Robinson, L. Havela, V. Sechovsky, P. Svoboda, H. Nakotte, K. Prokès, F.R. de Boer, A. Seret, J.M. Winand, J. Rebizant, J.C. Spirlet, Phys. Rev. B 50 (1994) 6792.
[14] J. Rodriguez-Carvajal, Powder Diffraction, Satellite Meeting of the 15th Congress of IUCr, Toulouse, France, 1990, p. 127.
[15] V.F. Sears, Neutron News 3 (1992) 26.
[16] P.J. Brown, in: A.J.C. Wilson (Ed.), International Tables for Crystallography, vol. C(4.4.4), Kluwer Academic, Dordrecht, 1970.
[17] G.M. Sheldrick, in: SHELX 76, Program for Crystal Structure Determination, University of Cambridge, England, 1976.
[18] F. Fourgeot, P. Gravereau, B. Chevalier, L. Fournès, J. Etourneau, J. Alloys Compounds 238 (1996) 102.
[19] R.A. Robinson, A.C. Lawson, K.H.J. Buschow, F.R. de Boer, V. Sechovsky, R.B. Von Dreele, J. Magn. Magn. Mater. 98 (1991) 147.
[20] D.D. Koelling, B.D. Dunlap, G.W. Crabtree, Phys. Rev. B 31 (1985) 4966.
[21] L.M. Sandratskii, J. Kübler, Physica B 217 (1996) 167.
[22] F. Bourée, B. Chevalier, L. Fournès, F. Mirambet, T. Roisnel, V.H. Tran, Z. Zolnierek, J. Magn. Magn. Mater. 138 (1994) 307.
[23] H. Nakotte, A. Purwanto, R.A. Robinson, K. Prokès, J.C.P. Klaasse, P.F. de Chatêl, F.R. de Boer, L. Havela, V. Sechovsky, L.C.J. Pereira, A. Seret, J. Rebizant, J.C. Spirlet, F. Trouw, Phys. Rev. B 53 (1996) 3263.
[24] V.H. Tran, Z. Zolnierek, F. Bourée, T. Roisnel, J. Magn. Magn. Mater. 161 (1996) 270.
[25] R.A. Robinson, A.C. Lawson, V. Sechovsky, L. Havela, Y. Kergadallan, H. Nakotte, F.R. de Boer, J. Alloys Compounds 213–214 (1994) 528.